J Mater Sci (2011) 46:6664–6672
DOI 10.1007/s10853-011-5619-0

Effect of moisture absorption on the micromechanical behavior of carbon fiber/epoxy matrix composites

J. I. Cauich-Cupul · E. Pérez-Pacheco · A. Valadez-González · P. J. Herrera-Franco

Received: 17 March 2011 / Accepted: 9 May 2011 / Published online: 24 May 2011

Abstract Carbon fiber/epoxy material in the form of a single fiber unidirectional composite was subjected to controlled humidity environments. Moisture uptake in polymer composites has significant effects on the mechanical properties of the matrix as well as on the final performance of the composite material. Diminishing of the mechanical properties of the matrix is attributed to a decrease of its glass transition temperature (T_g). The quality of the fiber–matrix interphase was assessed using the single fiber fragmentation test and the fiber-fragment length, considered as an indicator of interfacial quality. In order to measure the fiber fragment lengths and indentify failure mechanism at the interface optical observation and acoustic emission technique were used. The speed of propagation of an acoustic wave in the material was also determined. A comparison is made of interfacial shear strength values determined by acoustic emission and optical techniques. Excellent agreement between the two techniques was obtained. By means of a micromechanical model, it was possible to determine from the fragmentation lengths a measure of the interfacial shear strength between the fiber and the matrix. The role of moisture uptake swelling of the matrix on the residual stresses is considered to be important when considering the effect deterioration of interfacial shear properties. Both the contribution of the radial stresses and the mechanical component of fiber–matrix adhesion are seen to decrease rapidly for higher moisture contents in the matrix and/or interface.

J. I. Cauich-Cupul · A. Valadez-González · P. J. Herrera-Franco (✉)
Centro de Investigación Científica de Yucatán, Unidad de Materiales, Calle 43, No. 130, Colonia Chuburná de Hidalgo, C.P. 97200 Mérida, YUC, México
e-mail: pherrera@cicy.mx

E. Pérez-Pacheco
Instituto Tecnológico de Mérida, Av. Tecnológico km. 4.5 S/N C.P. 97118, Mérida, YUC, México

Introduction

There exists experimental evidence about the degradation of organic type matrices and of the fiber–matrix interface because of the absorption of moisture [1]. Water absorption in a polymer, is generally accompanied by a volumetric expansion (swelling) that modifies the state of residual stresses in the composite material. This swelling could be attributed to factors such as: (a) The hydrophobic character of the engineering fibers [2]; (b) to the difference of physico-chemical and mechanical properties between fiber and matrix [3]; (c) to a plasticization of the composite, evidenced by its softening and a decrease of its glass transition temperature (T_g) [1, 4]. One of the effects of water absorption is the degradation of the interfacial region between the fiber and the matrix (interphase) by hydrolysis [5] and chemical attack that results in a reduction of the stress transfer between fiber and matrix [6]. Drzal et al. [7] demonstrated that the interface in a carbon fiber–epoxy matrix composite material is degraded by moisture and that such degradation has both reversible and irreversible effects, depending on the temperature of hygrothermal exposure, the applied mechanical stress and the type of surface treatment on the fiber. On the other hand, silane-coupling agents posses organic functional groups that can react with a second functional group of the matrix, forming an inorganic layer with a coupling effect with the fiber.

These materials are capable of improving the interaction between the fiber and the matrix, improving the interfacial shear strength and consequently, the mechanical properties of the composite material exposed to either, humid or dry environments. The experimental methods used in the last few years to characterize the interphase in composite materials have focused on the determination of the level of adhesion between the fiber and the matrix and on the interfacial failure modes. Mechanically, the interphase has been characterized as a function of a single parameter: the interfacial shear strength between fiber and matrix. The method used for the determination of the interfacial shear strength is the single fiber fragmentation test (SFFT). Traditionally, this fragmentation process is observed and analyzed from the measurement of the final fiber fragment length by optical methods. A second alternative that has been used to determine the fiber fragment lengths is the acoustic emissions technique. This technique offers the advantage over the optical method that it can be used even with opaque matrices, where the points of rupture of the fibers are not visible and direct observation is not possible [8].

The acoustic emissions technique is based on the fact that when a material is stressed, some failure mechanism is activated, part of the total strain energy is dissipated as a wave that propagates from the failure source through the medium. The strain energy changes and the sudden movement produces a stress wave that propagates through the material. When the applied stress increases, many of these emissions are generated and three different failure modes can be identified in polymer matrix composites (breakage, matrix cracking and fiber–matrix debonding). The stress wave propagation is recorded using a highly sensitive piezoelectric sensor, and the signals from one or more sensors are amplified and measured for their interpretation [9, 10, p. 493]. In the single fiber fragmentation test, failure of the embedded fiber will produce a sudden change in geometry also resulting on the generation of acoustic wave propagation through the specimen. The fiber fragment length measurement by the acoustic emissions technique is based on the measurement of the speed of propagation of the signal as an acoustic wave through the medium. Such speed could be influenced by geometrical parameters, the frequency of the emitted signal, as well as the deformation of the material. The acoustic emission signal containing detailed information can be detected by one or more sensors and can be used to locate the fiber fragment lengths.

In this article, the effect of moisture absorption in a matrix and/or interphase on the level of fiber–matrix adhesion is studied for three different levels of adhesion. The measurements were performed using the single fiber fragmentation test complemented by optical methods and acoustic emission techniques for the measurement of fiber-fragment lengths.

Materials

A diglycidyl ether of bisphenol A (DGEBA)-based epoxy resin (Epon 828 from Shell Chemical Company) was used as matrix. Metaphenilene diamine (mPDA) ACS reagent grade was used as a curing agent, and, 3-glycidoxy propyl trimetoxy silane ACS reagent grade from Aldrich Chemical Co as a coupling agent. Intermediate modulus carbon fibers, IM7 12 K from Hexcel Co. with an average fiber diameter of 7.0 μm and two different surface conditions were used throughout this study: (1) unsized fibers (untreated, UT) resulting from the commercial sizing removal with a nitric acid treatment, (2) washed fibers and (3) subsequently treated with a silane coupling agent (ST).

Experimental procedures

Fiber surface treatments

The single fiber fragmentation test coupons were prepared using the IM7 carbon fiber with three different surface treatments. The nomenclature used for each fiber surface treatment is the following: (1) IM7, refers to the carbon fiber, "as received"; (2) IM7 + Silane, refers to the IM7 fiber whose commercial sizing was removed and treated with the selected silane coupling agent, and (3) IM7 + HNO3 + Silane, refers to the IM7 fiber, but treated with nitric acid and the silane coupling agent after removal of the commercial sizing. For the removal of the commercial sizing, the fibers were immersed and refluxed in methyl-ethyl ketone in a Kettle reactor during 12 h. Afterwards, they were washed with acetone, and then with distilled water. Finally, they were dried in an oven at 120 °C for 24 h. For the silane coupling agent surface treatment, distilled water and methanol were first thoroughly mixed (50% v/v), and the pH of the solution measured and adjusted to 4.5 using a diluted solution of acetic acid. Then, the silane coupling agent was added to a concentration of 0.1% (w/w) and agitated for two additional hours. Then the fibers were immersed in the solution for 1 h, and then they were dried in an oven at 120 °C during 1 h. The nitric acid fiber surface treatment was applied to the carbon fibers after removal of the commercial sizing. The fibers were immersed in the acid (70% purity) and refluxed for 6 h in a Kettle reactor. Afterwards, the fibers were washed in distilled water and refluxed for 2 h in the reactor to remove any traces of the acid and then, they were dried in an oven at 120 °C for 2 h.

SFFT coupon preparation

Epoxy–matrix test coupons for the single fiber fragmentation test were fabricated by a casting method with the aid of a silicone room temperature vulcanizing eight-cavity mold. Standard ASTM 50.8 mm long dogbone specimen cavities with a 3.175 mm wide by 1.587 mm thick by 25.40 mm long gauge section are molded into a 76.20 × 203.20 × 12.70 mm silicone piece. Single fibers ~150 mm in length are selected by hand from a fiber bundle. Single filaments are carefully separated from the fiber tow without touching the fibers, except at the ends. Once selected, a filament was mounted in the mold and held in place with a small amount of rubber cement at the end of the sprue. The assembly was transferred to an oven (Squaroid, Model 3608-5, for 2 h at 75 °C and 2 h at 125 °C) until the curing cycle was completed. The specimens were tested in uniaxial tension using a microstraining machine (MINIMAT) capable of applying enough load to the tensile coupon and fitted with a 1000 N load cell. The samples were tested using a crosshead speed of 0.02 mm/min. The load was applied and the inspection of the fiber fragmentation processed was assessed every 0.5 mm elongation intervals by counting the number of fragments. This processed was repeated until the number of fiber fragments did not increase with an increase of the applied load. At this point, the test was stopped and the resulting fiber fragments were measured using an optical caliper Image XR2000. The image of the fibers was magnified using a 50× Olympus microscope objective lens (Neo Plan50) fitted to a TV camera which was connected to a TV monitor. In order to assess the failure process, a transmitted light polarizing microscope was configured such that there was one polarizer below and one above the test coupon for observation of the photoelastic pattern evolution as a result of the induced birefringence in the matrix.

Moisture conditioning

The samples were conditioned to several relative humidity controlled environments (25, 55, and 95%) at a constant temperature of 25 °C, until ready for the mechanical and interfacial characterization. Air-tight sealed glass chambers were used as conditioning chambers. The different relative humidity environment chambers were obtained using several saturated salts. These salts were selected to obtain the different relative humidity atmospheres according to ASTM E104-51 and E104-85 standards, [11, 12]. A digital hygrometer was placed inside each chamber in order to measure and continuously monitor the temperature and relative humidity inside each chamber. The weight gain of the test coupons after exposure to the selected relative humidity environments was measured as a function of time. The humidity content was estimated using the following equation [13, 14]:

$$M = \frac{M_{\mathrm{W}} - M_{\mathrm{d}}}{M_{\mathrm{d}}} \times 100\% \quad (1)$$

where M is the percentage of gained humidity, M_{w} is the weight of the wet sample, and M_{d} is the weight of the dry sample.

Determination of the speed of propagation of the acoustic signal

The speed of propagation of the acoustic signal in the epoxy samples, before and after moisture exposure was measured utilizing two piezoelectric transducers (see sensors 1 and 2 in Fig. 1). Each transducer with an effective area of contact equal to 17.795 mm^2 was affixed to the tensile test coupon and to insure good contact, vacuum silicon grease was used. A notch, 0.5 mm deep was cut on one side of the coupon as a crack initiator. These two piezoelectric sensors were located at known distances from the notch. Sensor one was located at 4.88 mm from the notch and sensor two at 9.88 mm.

A tensile load was applied to the test coupon using a mini tensile testing device (MINIMAT) equipped with a load cell of 1000 N. The cross-head speed was fixed at 0.02 mm/min. Upon crack initiation, the stress wave propagating as an acoustic signal was recorded and analyzed using commercial software called MITRA™. The difference in the time of arrival (Δt) of the acoustic signal to each of the sensors, and corresponding to the first event of crack growth was recorded (see Figs. 2, 3). Then the speed of propagation was calculated using Eq. 2:

$$V = \frac{\Delta d}{\Delta t} \quad (2)$$

where V is the average speed of propagation of the acoustic signal, Δd is the difference of distance between the location

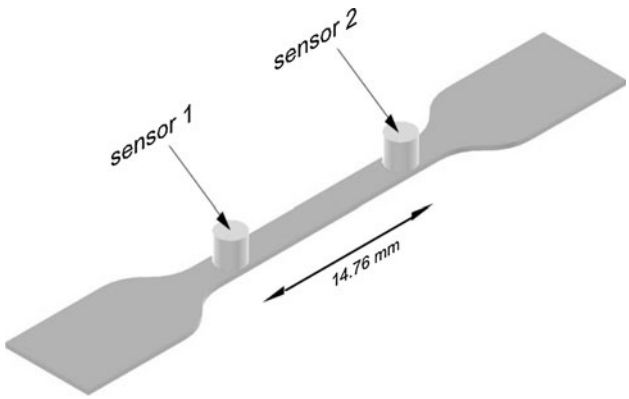

Fig. 1 Test coupon for the determination of the speed of propagation of the acoustic signal

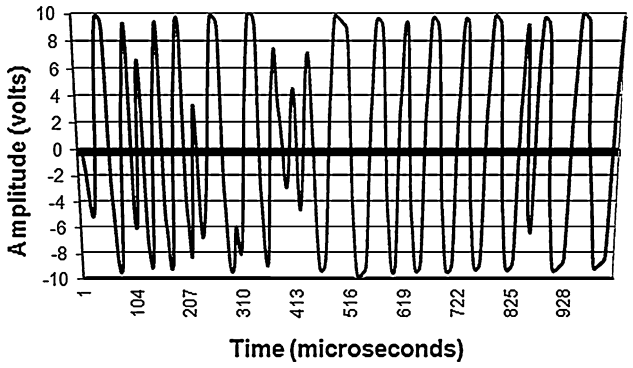

Fig. 2 Graph of signal amplitude versus time of arrival to sensor 1

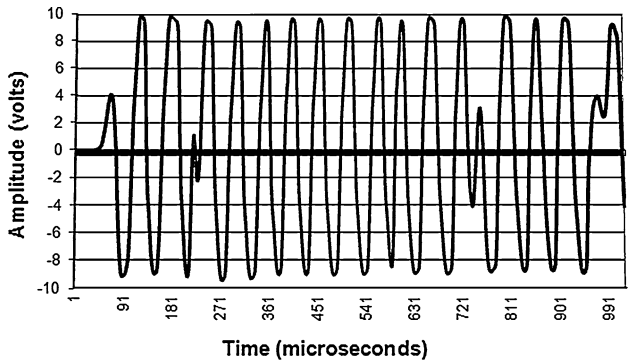

Fig. 3 Graph of signal amplitude versus time of arrival to sensor 2

of the sensors and the notch in the test coupon. This procedure was repeated for the test coupons conditioned at the selected relative humidity.

Determination of Young's modulus using acoustic signals

The speed of propagation of a wave in a medium is a function of the properties of the material itself and geometrical parameters, dominating frequency of the emitted signal, and most important, the deformation produced in the material [15]. From Newton's second law of motion:

$$\rho \frac{\partial^2 u}{\partial t^2} = E \frac{\partial^2 u}{\partial x^2} \tag{3}$$

where u is the displacement of a differential element in the x-direction, ρ is the mass density of the sample, E is Young's modulus, and t is time. This equation corresponds to the propagation of longitudinal waves along the material with velocity equal to $\sqrt{E/\rho}$. The solution of Eq. 3 may be written as:

$$u = f(c_0 t - x) + F(c_0 t + x), \tag{4}$$

where $c_0 = \sqrt{E/\rho}$. F and f are arbitrary functions depending on the initial conditions. The function f corresponds to a wave traveling in the direction of increasing x, while, the function F corresponds to a wave traveling in the opposite direction. With further mathematical manipulation, it can be shown that Eq. 4 can be expressed as:

$$\sigma_{xx} = \left(\frac{E}{c_0}\right)\frac{\partial u}{\partial t} = \rho c_0 \frac{\partial u}{\partial t} \quad \text{or} \quad E = \frac{\sigma^2}{V^2}\rho, \tag{5}$$

where σ_{xx} is the stress component along the axis of wave propagation, V is the speed of the particle. Equation 5 shows that there exists a linear relationship between the stress at any point in the material and the speed of the particle, being this relationship between them, the corresponding impedance, ρc_0.

Measurement of fiber fragment length using acoustic emissions

The fiber fragment lengths while performing the single fiber fragmentation test were also measured using the acoustic emissions arising from the fiber fracture, and both the interfacial crack growth and the matrix-crack growth. The acoustic emissions were detected using the same two piezoelectric transducers (see Fig. 4). Each transducer with an effective area of contact equal to 17.795 mm^2 was affixed to the tensile test coupon and to insure good contact, vacuum silicon grease was used. The distance between transducers was fixed at 14.76 mm using a template especially built to accurately position them always at the same distance. A tensile load was applied to the test coupon using a mini tensile testing device (MINIMAT) equipped with a load cell of 1000 N. The cross-head speed was fixed at 0.02 mm/min. Upon crack initiation, the stress wave propagating as an acoustic signal was recorded and analyzed using commercial software called MITRA™. A threshold value of 40 dB was used to isolate the high sensitivity transducers from external noise. The acoustic signals were pre-amplified using preamplifiers whose gain was also set to 40 dB. A frequency range from 10 to 1200 kHz was used in the test and the speed of event detection was set to 10 MHz in a synchronized mode. A

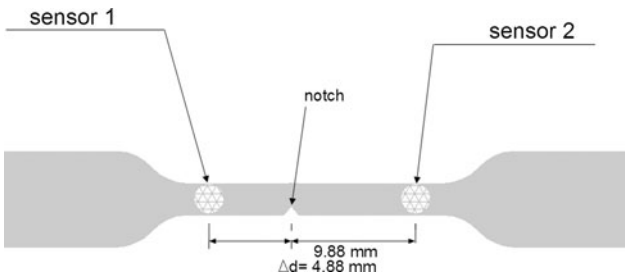

Fig. 4 Test coupon for the determination of the fiber fragment lengths using the acoustic emissions technique

simple algorithm incorporating the average wave speed in the epoxy (or any other matrix), the distance between the two receiving transducers, the offset distance between one specific receiving transducer and the fixed grip, time intervals and the corresponding strains was used to obtain the location of the fiber breaks, the fiber fragment lengths, and fiber aspect ratios. In the case of the acoustic emissions fiber-fragment measurement, the fragmentation process was monitored only as a function of the acoustic signals being monitored, that is, once the load was applied, the test was ended when no more signal were being registered by the system. The strain in the sample was also continuously monitored to avoid sample fracture.

Results and discussion

Figure 5 shows isotherms of absorbed moisture as a function of time for the different relative humidity atmospheres. For the 25% RH, the amount of gained weight stabilizes at ~0.15% after 90 days of exposure. For the 55% RH, a larger amount of moisture is gained during the first 20 days and then it stabilizes at a maximum of 1% after 90 days of exposure. For the 95% RH, the maximum amount of absorbed water of ~2% was achieved after 290 days of exposure. It was observed that the moisture absorption rate was high at the beginning of the exposure of the samples, especially during the first 20 days; afterwards, the absorption rate slowly decreased until 90 days of exposure and then it stabilized to a maximum of 1%. Only for the 95% RH environment, the absorption rate rapidly increased during the first 20 days, and then it stabilized to a moisture gain of ~2%, after 90 days.

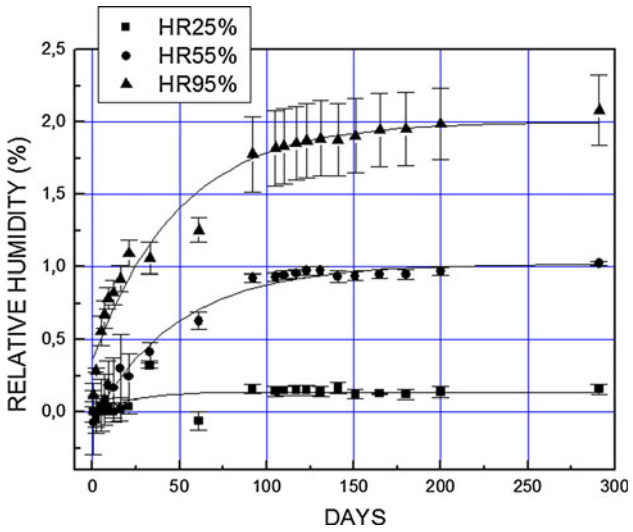

Fig. 5 Isotherms of moisture absorption for the epoxy resin

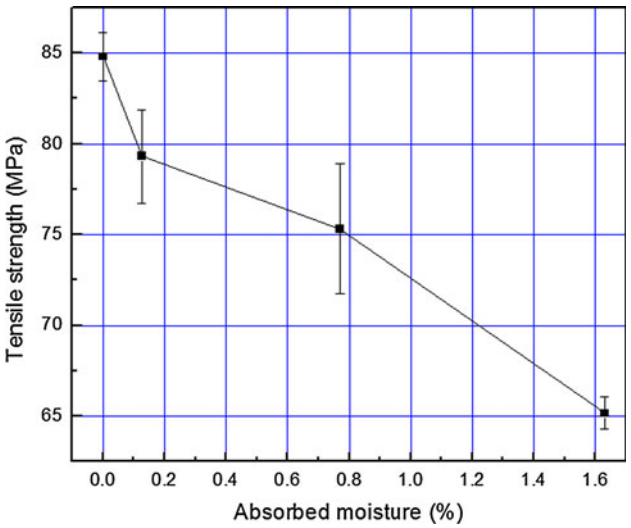

Fig. 6 Tensile strength as a function of absorbed moisture

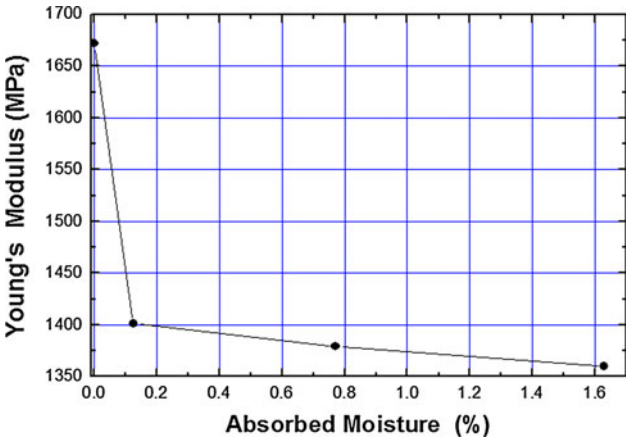

Fig. 7 Young's modulus of the epoxy matrix as a function of absorbed moisture

Figures 6 and 7 show the tensile strength and the elastic modulus of the epoxy matrix as a function of absorbed moisture during 290 days, respectively. The decrease of the resin tensile strength notoriously decreases when the amount of absorbed moisture increases. For the highest moisture gain, such tensile strength decreases from 85 to 65 MPa, that is, a loss of ~23.5%. As shown in Fig. 7, the decrease of the matrix rigidity of ~16.4% is notorious after moisture absorption of 0.1%. Such rate of change is high during the first 20 days of exposure, and then it slowly decreases with higher moisture gain.

The effect of moisture absorption on the mechanical properties of the polymer is attributed to a plasticization as evidenced by a reduction of its glass transition temperature T_g [4, 5]. The degradation of the mechanical properties of epoxy polymers due to moisture absorption is associated to the plasticization and to a micromechanical damage

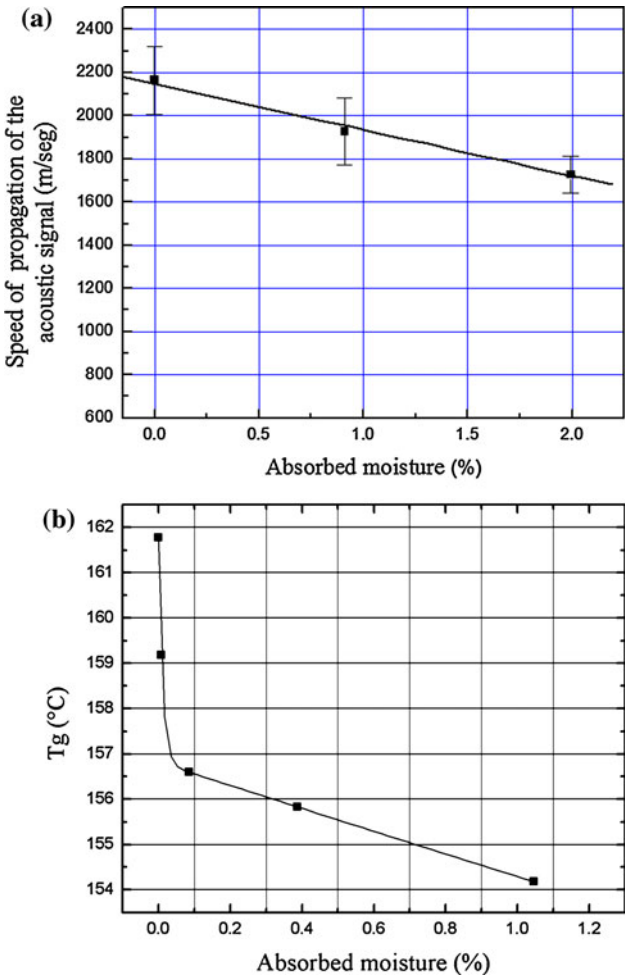

Fig. 8 **a** Speed of propagation of the acoustic signal as a function of absorbed moisture; **b** decrease of the T_g of the epoxy matrix as a function of absorbed moisture

induced by the absorbed moisture [16, 17]. The decrease of the properties caused by the interactions between the polymer and the absorbed water is a rapid and powerful phenomenon with an apparent stability during the first stage of moisture diffusion. Afterwards, the tendency of the polymer network to absorb moisture decreases and a relative stabilization is observed [18, 19]. As mentioned before, the speed of propagation of an acoustic signal in a medium is a function of the physico-chemical properties of the material. As shown in Fig. 8a, for an epoxy resin after exposure at a 95% RH, a 2% moisture absorption results in a decrease of acoustic signal propagation speed of approximately a 22.72% as compared to a 0% moisture absorption. Then, the decrease of the stiffness of the material results in a damping of the acoustic signal as it travels in the material. This damping should be related to the viscoelastic behavior of the matrix, since its T_g is decreasing (Fig. 8b).

The fiber-critical length is very important for the calculation of the interfacial shear strength, especially when

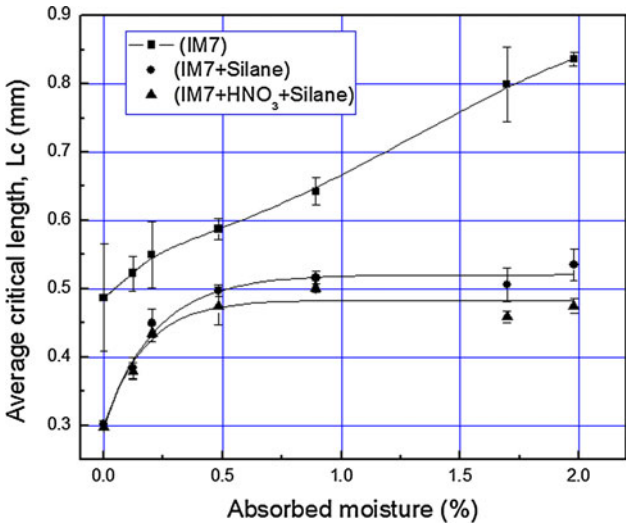

Fig. 9 Average fiber critical length as a function of absorbed moisture as measured by the optical method

studying the degradation caused by hygrothermal exposures of the composite. Such fiber-critical length is considered an indicator of fiber–matrix adhesion level in the composite. Therefore, the interpretation of the change in the fiber critical length as a function of absorbed moisture clearly shows how this fiber–matrix adhesion is deteriorating because of moisture diffusion in the composite. As shown in Fig. 9, there is a notorious increment of the average L_c for the untreated carbon fiber (IM7) with increasing moisture content. The fiber-fragment length rate of change with absorbed moisture follows all three linear stages. The first stage is noticed up to a moisture content of $\sim$0.25%, and the second up to 0.85%. The third stage for higher moisture contents. Longer fragments were measured with higher amounts of absorbed moisture. However, when the fiber–matrix adhesion is changed, either with the new silane treatment or the nitric acid activated and silane-treated fiber, two different stages of fiber-fragment length as a function of absorbed moisture are observed. There is a high rate of change up to a 0.5% of absorbed moisture and afterwards, no notorious change is observed, even for high moisture contents in the matrix. No notorious difference is observed in the critical length behavior when the fiber is treated with nitric acid. Similar trends of the change of average critical length was noticed when it was measured using the acoustic emissions technique (see Fig. 10).

Swelling is a specific response to moisture diffusion in epoxy resins or composites based on them [20–23]. It is very important in both composites and adhesive joints, because it can significantly affect mechanical behavior by build-up of residual stress at and near interfaces. Hygroscopic swelling is mechanically similar to thermal expansion in that both are physical phenomena involving

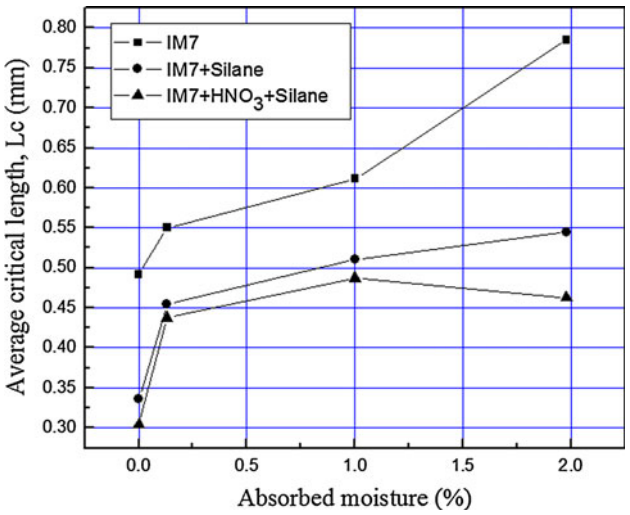

Fig. 10 Average fiber critical length as a function of absorbed moisture as measured by the acoustic emissions method

molecules equilibrating a larger distance apart as a result of temperature increase and moisture absorption, respectively.

In both, the magnitudes of expansion, ε_T and ε_M are given by: $\varepsilon_T = \alpha\Delta t$ and $\varepsilon_M = \beta\Delta M$, where α and β are the coefficients of thermal and moisture expansion coefficients, respectively, ΔT and ΔM are temperature and moisture gradients, respectively.

Whitney and Drzal [24] proposed an approximate closed form solution which predicts the axisymmetric stress distribution in a system consisting of a single broken fiber surrounded by an unbounded matrix, (Fig. 11). The approximate solution is based on knowledge of the basic nature of the stress distribution near the end of the broken fiber, represented by a decaying exponential function multiplied by a polynomial. Equilibrium equations and the boundary conditions of classical elasticity theory are exactly satisfied throughout the fiber and matrix, while compatibility of displacements is only approximately satisfied. The far-field solution away from the broken fiber end satisfies all the equations of elasticity. The model also includes the effects of expansional strains as a result of moisture and temperature. Axisymmetric behavior was assumed in the development of the model.

A relationship is obtained for the axial normal stress σ_x in the fiber (see Fig. 11):

$$\sigma_x = \left[1 - (4.75\bar{x} + 1)e^{-4.75\bar{x}}\right]A_1\varepsilon_0 \tag{6}$$

where $\bar{x} = x/L_c$, ε_0 is the applied far-field strain and A_1 is a constant dependent on material properties, thermal strains, and the applied far-field strain. It can be noticed that σ_x is independent of the fiber radius. The critical length L_c is defined such that the axial stress recovers 95% of its far-field value, that is:

$$\sigma_x(L_c) = 0.95A_1\varepsilon_0$$

The interfacial shear stress is given by the Eq. 7:

$$\tau_{xr}(\bar{x}, r) = -4.75\mu A_1\varepsilon_0\bar{x}e^{-4.75\bar{x}} \tag{7}$$

where $(0 \le r \le R)$.

$$\mu = \sqrt{\frac{G_m}{E_{1f} - 4v_{12f}G_m}} \tag{8}$$

E_{1f} denotes the axial elastic modulus of the fiber, whereas v_{12f} is the longitudinal Poisson's ratio of the fiber, determined by measuring the radial contraction under an axial tensile load in the fiber axis direction, and G_m, denotes the matrix shear modulus. It should be noted that the negative sign in the expression for the shear stress is introduced to be consistent with the definition of an interfacial shear stress in classical elasticity theory. The radial stress at the interface is computed according to Eq. 9 by:

$$\sigma_r = \frac{2k_fG_m}{(k_f + G_m)}A_2\varepsilon_0 + \mu^2A_1(4.75\bar{x} - 1)\varepsilon_0 e^{-4.75\bar{x}} \tag{9}$$

Constants A_1 and A_2 (see Eqs. 10, 11) are dependent on material properties, thermal strains and the applied far-field strain and μ is calculated by Eq. 8. Numerical results are normalized by σ_0, which represents the far-field fiber stress in the absence of expansional strains. In particular, $\sigma_0 = A_3\varepsilon_0$

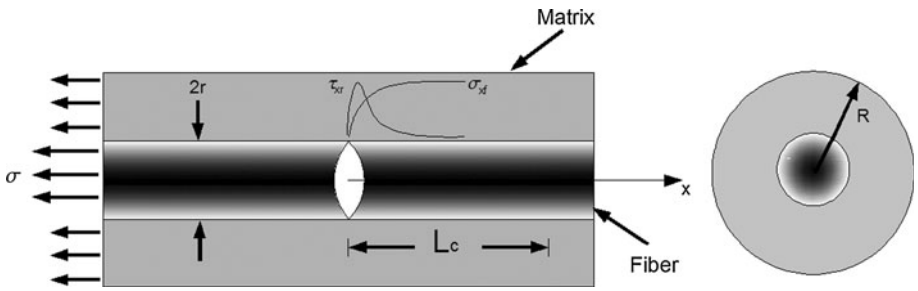

Fig. 11 Micromechanical model for the single fiber fragmentation process

The constants A_1, A_2, and A_3 are given by:

$$A_1 = \left\{ E_{1f}\left(1 - \frac{\bar{\varepsilon}_{1f}}{\varepsilon_0}\right) + \frac{4k_f G_m v_{12f}}{(k_f + G_m)}\left[(v_{12f} - v_m) + \frac{(1+v_m)\bar{\varepsilon}_m -}{\varepsilon_0}\right.\right. \tag{10}$$

$$A_2 = (v_{12f} - v_m) + \frac{[(1+v_m)\bar{\varepsilon}_m - \bar{\varepsilon}_{2f} - v_{12f}\bar{\varepsilon}_{1f}]}{\varepsilon_0} \tag{11}$$

$$A_3 = E_{1f} + \frac{4K_f v_{12f} G_m (v_{12f} - v_m)}{K_f + G_m}. \tag{12}$$

And, $\bar{x} = x/L_c$ is the applied far-field strain, K_f calculated according to Eq. 13 by:

$$K_f = \frac{E_m}{2\left(2 - \frac{E_{2f}}{2G_{2f}} - \frac{2v_{12f}^2 E_{2f}}{E_{1f}}\right)} \tag{13}$$

where the thermal strains are indicated by overbars, and E_{2f}, G_{2f}, and K_f are the radial elastic modulus, the shear modulus in the plane of the cross-section and the plane-strain bulk modulus of the fiber, respectively.

The material properties used are shown in Table 1. The reference moisture value used was a 25% RH and is referred to as 0%.

As seen in Fig. 12, the moisture uptake influences the stress distribution along the fiber–matrix interface. For the untreated fiber, the maximum axial stress is achieved a point located farther away from the point of fiber break. Thus, a longer fiber fragment length could be expected. In the case of the silane-treated fiber, the maximum axial stress occurs at a point located closer to the fiber break. Here, a shorter fiber fragment could be expected. This is consistent with the measured fiber fragment lengths measured experimentally.

Also, a higher shear interfacial shear stress is observed for the silane-treated fiber, and the distribution along the fiber fragment decreases more rapidly at points located far away from the break (see Fig. 13).

Furthermore, swelling due to moisture uptake can be used to explain the fiber–matrix interface degradation. For the 0% moisture uptake, the residual stress in the radial arising from both curing and thermal coefficients of expansion of direction between fiber and matrix and the expansional strains due to moisture uptake decrease considerably for higher moisture contents.

Both thermal and moisture strains decrease and this should result in a reduction of the radial stress component (shown in Fig. 14), which is considered to contribute to the frictional interfacial shear stress component. In the case of the untreated fiber, since no physico-chemical interactions exist between fiber and matrix, such mechanical component to adhesion is important. In the case of the silane-treated fiber, the existence of covalent bonds between the fiber and matrix explain the behavior of the constant fiber fragment lengths, even at high moisture contents.

Table 1 Fiber and matrix material properties

Property	Epoxy resin			IM7
	0%	0.9%	2%	
E_1 (GPa)	1.435	1.318	1.303	241
E_2 (GPa)	1.435	1.318	1.303	21
v_{12}	0.35	0.35	0.35	0.25
G_{23} (GPa)		0.53		8.3
α_1 (10^{-6}°C^{-1})		68		−11
β_1 (10^{-6}°M^{-1})		0.33		–

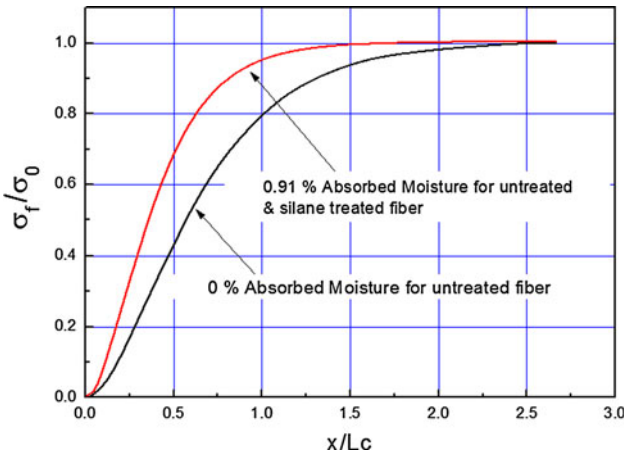

Fig. 12 Interfacial fiber axial stress distribution for untreated and silane-treated fiber for two different relative humidity environments

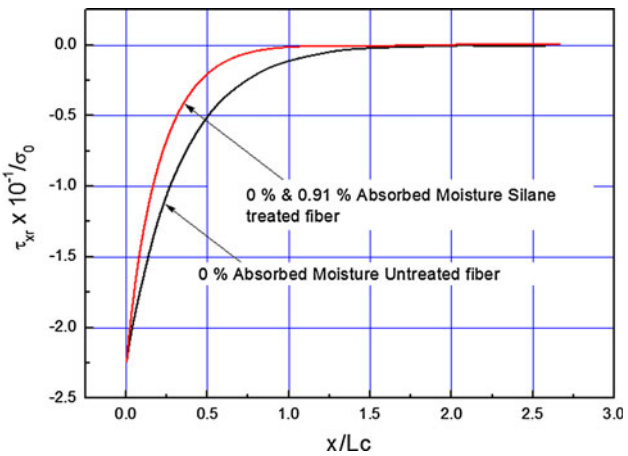

Fig. 13 Interfacial shear stress distribution for untreated and silane-treated fiber for two different relative humidity environments

Conclusions

Moisture uptake in epoxy/carbon fiber composite results in a detrimental effect on the mechanical properties of the

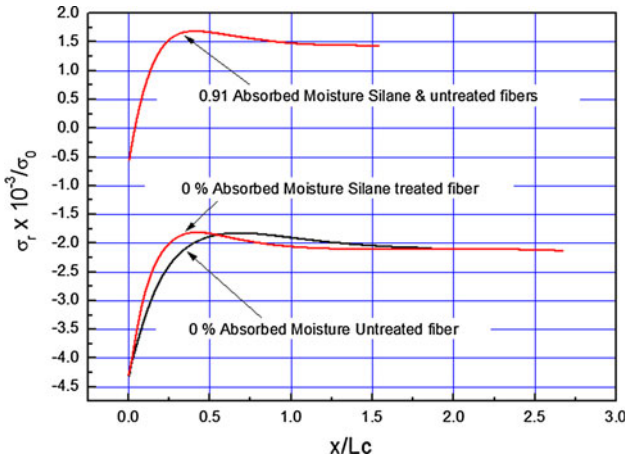

Fig. 14 Interfacial radial Interfacial shear stress distribution for untreated and silane-treated fiber for two different relative humidity environments stress distribution for untreated and silane-treated fiber for two different relative humidity environments

matrix, and this deterioration is attributed to a decrease of its glass transition temperature. The quality of the fiber–matrix interface was assessed using the single fiber fragmentation test and the fiber-fragment length, considered as an indicator of interfacial quality indicated a continuous deteriorating effect of moisture uptake. The fiber fragment lengths were measured using an optical observation system and the results compared to an acoustic emissions technique. In order to use the second technique, the speed of propagation of an acoustic wave in the material was determined. Excellent agreement between the two techniques was obtained. Also, a micromechanical model was used to explain the observed fiber-fragment lengths. The role of moisture uptake swelling of the matrix on the residual stresses is considered to be important when considering the deterioration of interfacial shear properties. The contribution of the radial stresses is seen to decrease rapidly and the mechanical component of the fiber–matrix adhesion also decreases rapidly for higher moisture contents in the matrix and/or interface.

Acknowledgements The authors wish to express the financial support from Consejo Nacional de Ciencia y Tecnología given through grant # 31272-U and for the scholarships granted to Mrs. Emilio Pérez Pacheco and Mr. Javier I. Cauich Cupul.

References

1. Xiao GZ, Shanahan MER (1997) J Polym Sci B 3:2659
2. Pomies F, Carlsson LA (1994) J. Compos Mater 28:22
3. Adams DF (1986) A micromechanies analysis of the influence of the interface on the performance of polymer matrix composites. In: Proceedings of the American Society for composites, lst technical conference, 7–9 Oct. Technomic publishing, Dayton, p 207
4. Chateauminois A, Chabert B, Soulier JP, Vincent L (1995) Polym Comp 16:288
5. Soles CL, Chang FT, Gidley DW, Yee AF (2000) J Polym Sci B 38:776
6. Drzal LT, Rich MJ, Koenig MF (1985) Adhesion 18:49
7. Spragg CJ, Drzal LT (1996) Fiber, matrix and interface properties. ASTM STP no 1290. American Society for Testing and Materials, West Conshohocken
8. Netravali AN, Li ZF, Sachse WH, Wu HF (1990) In: Buckley JD (ed) Third conference on advanced engineering fibers and textile structure for composites. NASA conference publication 3082, Hampton, VA
9. Park JM, Chong EM, Dong JY, Lee JH (1998) Polym Comp 19:747
10. Nielsen LE, Landel RF (1994) Mechanical properties of polymers and composites. CRC Press, New York
11. ASTM (1985) Maintaining constant relative humidity by means of aqueous solutions. Book of ASTM standards, part 6. ASTM Designation E 104-85. American Society for Testing Materials, Philadelphia
12. Mijovic J, Lin KF (1985) J Appl Polym Sci 30:2527
13. Vanlandingham MR, Eduljee RF, Gillespie JW (1999) J Appl Polym Sci 71:787
14. Xiao GZ, Shanahan MER (1998) J Appl Polym Sci 69:363
15. Kolsky H (1963) Stress waves in solids. Dover Publications Inc., New York
16. Lu MG, Shim MJ, Kim SW (2001) J Appl Polym Sci 8:2253
17. Nogueira P, Ramirez C, Torres A, Abad MJ, Cano J, Lopez J, Lopez-Bueno I, Barral L (2001) J Appl Polym Sci 80:71
18. Rao V, Drzal LT (1991) Polym Compos 12:48
19. Adamson MJ (1980) J Mater Sci 15:1736. doi:10.1007/BF00550593
20. Jackson ML, Love BJ, Hebner SR (1999) J Mater Sci Mater Electron 10:71
21. Xu ZR, Ashbee KHG (1994) J Mater Sci 29:394. doi:10.1364/AO.29.000394
22. El-saad L, Darby MI, Yates B (1989) J Mater Sci 24:1653. doi:10.1007/BF01105687
23. Ebrahimzadeh PR, Mcqueen DH (1998) J Mater Sci 33:1201. doi:10.1023/A:1004373525437
24. Whitney JM, Drzal LT (1987) In: Johnston NJ (ed) ASTM STP 937 ASTM Committee D-30 on high modulus fibers and their composites, Philadelphia, USA